Core−Shell Nanopillars of Fullerene C_{60}/C_{70} Loading with Colloidal Au Nanoparticles: A Raman Scattering Investigation

Zhixun Luo,[†,‡] Yong Sheng Zhao,[†] Wensheng Yang,[§] Aidong Peng,[†] Ying Ma,[†] Hongbing Fu,[†] and Jiannian Yao*[,†]

Beijing National Laboratory for Molecular Science (BNLMS), Institute of Chemistry, Chinese Academy of Sciences, Beijing 100190, P.R. China, Graduate School of the Chinese Academy of Sciences, Beijing, 100049, P. R. China, and College of Chemistry, Jilin University, Changchun 130012, P. R. China

Received: April 29, 2009; Revised Manuscript Received: July 15, 2009

High-density ordered core−sheath nanopillars of fullerene C_{60}/C_{70} loading with colloidal Au nanoparticles were fabricated with a template method. The anodic aluminum oxide (AAO) template was first imbedded with the fullerene C_{60}/C_{70} molecules and then followed by a pressure-difference approach for Au colloid. High-quality surface-enhanced Raman scattering (SERS) spectra of fullerene C_{60}/C_{70} were obtained. The spectra show intense SERS signals with a fluorescence-free background, even with a 514 nm excitation at which the normal Raman of fullerene C_{60}/C_{70} present poor signal-to-noise. The assembly of the fullerene C_{60}/C_{70} on the inner walls of the AAO pores along the Au nanopillars lead to fluorescence quenching; meanwhile, the high-density and ordered arrays of Au nanopillars contribute to surface plasmon resonance for the SERS effect.

1. Introduction

The unique structures and properties of fullerenes have made them ideal materials for nanoscaled electronic devices as well as fundamental researches.[1−3] Among the abundant investigations of fullerenes, well-prepared fullerene C_{60} thin films were widely studied with implications for device evaluations.[4] Recently, fullerene nanotubes have attracted the most considerable interest and have been found to be promising building blocks for electronic and optoelectronic devices.[5−7] Fullerene-functionalized metal nanoparticles and clusters have also been widely investigated and demonstrated to present unique spectroscopic properties and potential applications.[8−11] However, it is still not easy to prepare complex nanostructures based on functionalized fullerenes.

Recently, AAO templates have been applied to fabricate core−shell complex structures. For example, Lahav et al.[12] showed composite nanostructures of metal and polyaniline in two new variations of core−shell and segmented architectures; Daly and coworkers[13] investigated the nanocables consisting of magnetite nanowires surrounded by cobalt nanotube sheaths and cobalt nanowires surrounded by magnetite nanotube sheaths. Among them, several approaches have been found to be successful in gaining the coresheath structures in AAO pores, such as the sol−gel method.[14]

As one may know, when target molecules are located close to metal nanoparticles possessing surface plasmon resonance, the SERS effect may be achieved. For 1D fullerene C_{60} nanotubes loading Au nanoparticles, the excitation of the surface plasmon of Au nanoparticles will generate enhanced electromagnetic fields and provide the dominant contributions to the SERS spectroscopy.[15−18]

Herein, we achieved the high-density ordered arrays of core−shell nanopillars of $Au@C_{60}/C_{70}$ systems, shown as Scheme 1. As a result, we fabricated the structured nanoarchitectures obtained by employing a two-step approcah, infiltration, and then a pressure-difference method, and high-quality SERS spectra of fullerene C_{60}/C_{70} were obtained. It is notable that the observed high-quality SERS spectra show intense Raman signals with a fluorescence-free background, even with a 514 nm excitation by which normal Raman present poor signal-to-noise. Similar results were also obtained for the fullerene C_{70} system. These results give vivid evidence that the coincident and uniform assembled orientation of fullerene molecules along the Au nanorods led to fluorescence quenching and the high-density and ordered arrays of nanopillars, referred to as a unique SERS system, generate effective surface plasmon resonance to achieve the unique SERS.[19]

SCHEME 1: Sketch Map (a) of the $Au@C_{60}$ Nanopillar System and (b) from the Cross Section and (c) a Detailed Illustration for the Structure of $Au@C_{60}/C_{70}$ with the Support of AAO Frame

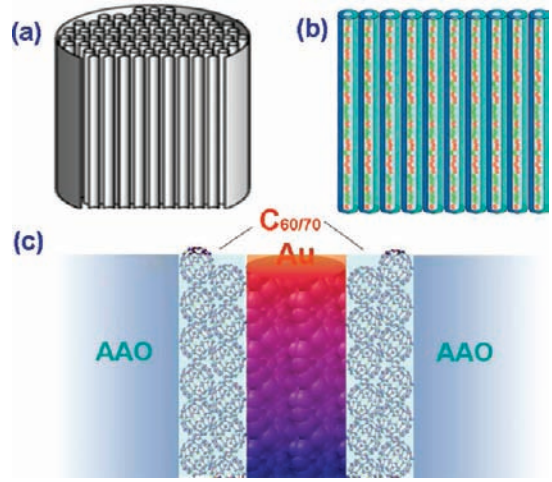

* Corresponding author.
† Institute of Chemistry, Chinese Academy of Sciences.
‡ Graduate School of the Chinese Academy of Sciences.
§ Jilin University.

10.1021/jp9041028 CCC: $40.75
Published on Web 08/04/2009

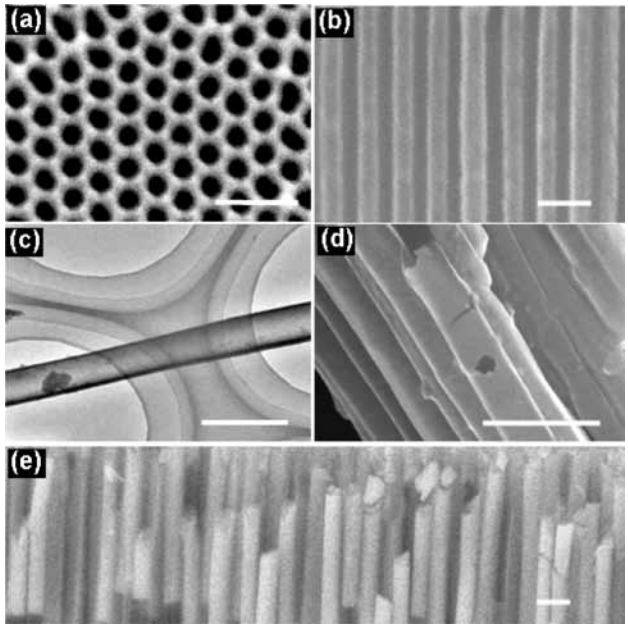

Figure 1. SEM images of the fabricated AAO templates from (a) the top view and (b) the cross section. (c) TEM and (d) SEM images of the as-prepared C_{60} nanotubes by infiltration method. (e) SEM image of the nanotubes observed from the cross section after the AAO frame was partially etched by NaOH solution. The dimension bars are 500 nm for all images.

2. Experimental Section

All chemicals used were of reagent grade unless otherwise specified. Au colloid was prepared according to the Fren's method.[20] $HAuCl_4 \cdot 3H_2O$ (1 mL, 1%) solution was added to 98 mL of deionized water and then heated to boiling. Then, sodium citrate aqueous solution (1 mL, 1%) was rapidly added. Wine-colored Au hydrosol was obtained after 15 min under vigorous stirring. The average diameter size of the as-prepared colloidal Au nanoparticles was about 16 nm.

The AAO templates were prepared according to a method described elsewhere.[16] Before anodization, aluminum foils (99.999% purity, Institute of Nonferrous Metal, Chinese Academy of Sciences) were first degreased in acetone and then annealed at 350 °C for 2 h. The annealed aluminum foils were etched in a mixture of perchloric acid and ethanol (1:4) for several minutes and then anodized at a constant voltage of 40 V in 0.40 M oxalic acid at 10 °C for 2 h. The surface alumina layer was removed in a mixture of phosphoric acid (6 wt %) and chromic acid (1.5 wt %), and the aluminum foils were reanodized under the same conditions for 2.5 h. A honeycomb structure of anodic porous alumina was then obtained (shown as Figure 1a,b) in which the pores were uniformly arranged in a close-packed hexagonal lattice, and they were continuous and parallel to each other. We could vary the diameter of the pores between 20 and 200 nm by controlling the experimental conditions.

The AAO templates (200 nm) were embedded with C_{60}/C_{70} molecules by soaking in a pyridine solution of saturated C_{60}/C_{70} (99.9% purity, purchased from Peking University), 2 min at a time, and then drying for 15 min. This process was repeated several times, and the templates were then dried at 100 °C in a nitrogen atmosphere, followed by a scouring and hole-blowing process.

The AAO templates embedded with C_{60}/C_{70} were then laid on a Buchner funnel with fritted disk (G4), connected to an accessory flask with side arm, kept under vacuum production, gradually dropped in Au hydrosol (2 min at a time), and then dried for 15 min. This process was repeated several times. They were at rest for a few minutes and were then repeated for several periods. They were then dried in nitrogen at 200 °C.

The AAO membrane then was carefully burdened by a physical after-treatment and a chemical treatment (NaOH solution, 3M). When dissolved, centrifugal separation made the pH value 7. The morphology and size of the sample were examined by field emission scanning electron microscopy (FESEM, Hitachi S-4300) and transmission electron microscope (TEM, JEOL JEM-1011). The Raman spectra were recorded on a Renishaw H13325 spectrometer using 514 nm excitation as well as on a Bruker model IFS-66 FT-Raman spectrometer with the 1064 nm excitation at 50 mW and a line resolution of 3 cm^{-1}.

3. Results and Discussion

The AAO templates fabricated here have narrow pore size distribution, shown as Figure 1a, with pores uniformly arranged in a regular hexagonal lattice and pore densities as high as 10^{11} pores/cm^2.[18,21,22] The pores are straight with a smooth inner surface (Figure 1b) and with diameters in a wide range of 20−200 nm. (See Figures S1 and S2 in the Supporting Information.) In the infiltration step, the templates were repeatedly dipped into a pyridine solution of C_{60}, and the solvent was allowed to dry before the next dipping. (See Figure S3 in the Supporting Information.) After several dip-and-dry cycles, the templates were heated to 450 °C and kept for 2 h under a nitrogen atmosphere and then cooled to room temperature. The diameter and length of the C_{60} nanotubes depend on the pore size and thickness of the AAO membrane used (ca. 5 μm). Figure 1c shows a TEM image of a single C_{60} nanotube after complete removal of alumina. Figure 1d refers to the several nanotubes separated on silicon piece, where they are sticking together. Figure 1e shows a SEM image of the as-prepared C_{60} nanotubes from cross section by selectively dissolving the template with 3 M NaOH solution. The well-ordered nanotubes grown from the membrane exhibit a straight alignment perpendicular to the substrate.

Actually, instead of the C_{60} nanotubes removed from the AAO template, we implanted Au nanoparticles (ca. 16 nm, Figure 2a) into the pores of the templates by pressure-difference after a surface treatment (ca. scouring and hole-blowing process; for details, see Figure S3 of the Supporting Information). Figure 2b gives a TEM image of the as-prepared Au@C_{60} nanorods, whereas Figure 2c refers to the SEM characterization of it before removing from AAO template, and Figure 2d shows the characters measured from the cross section. To make sure that the Au nanoparticles are implanted in the C_{60} nanotubes, a microtomy technique was operated from the cross section of the AAO-membrane-supported Au@C_{60} nanorodding arrays system. Figure 2e gives the SEM character of a single split Au@C_{60} nanorod from the cross section, whereas Figure 2f shows the correlative AFM image before split. It can be observed from Figure 2e that the Au nanoparticles were implanted into the AAO pores and aggregated and aligned along the wall of AAO holes.

After confirmation of the expected structures of Au@C_{60}, we focused on the characterization of the product by Raman spectra. Figure 3a gives the FT-Raman spectrum of solid C_{60} excited at 1064 nm, whereas Figure 3b shows Raman of C_{60} nanotube arrays supported on AAO templates, and the Raman spectrum of Au@C_{60} nanopillar arrays is addressed in Figure 3c. Rare Raman modes appeared in Figure 3b. Compared with Figure

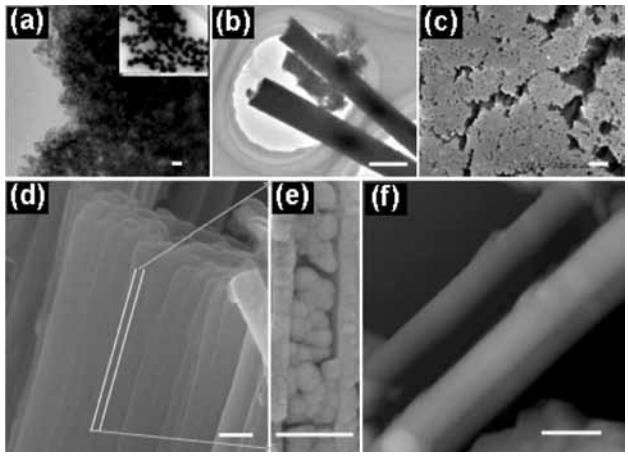

Figure 2. TEM images of (a) the fabricated Au nanoparticles and (b) the C_{60} nanotubes when implanted in the Au nanoparticles via pressure difference method. SEM images of the Au@C_{60} nanorods before removing from the AAO template measured from (c) the top view and (d) the cross section. (e) SEM image for the inner morphologies of a single Au@C_{60} nanorod split with microtomy technique. (f) AFM image of a few Au@C_{60} nanorods. The dimension bars are 200 nm for all.

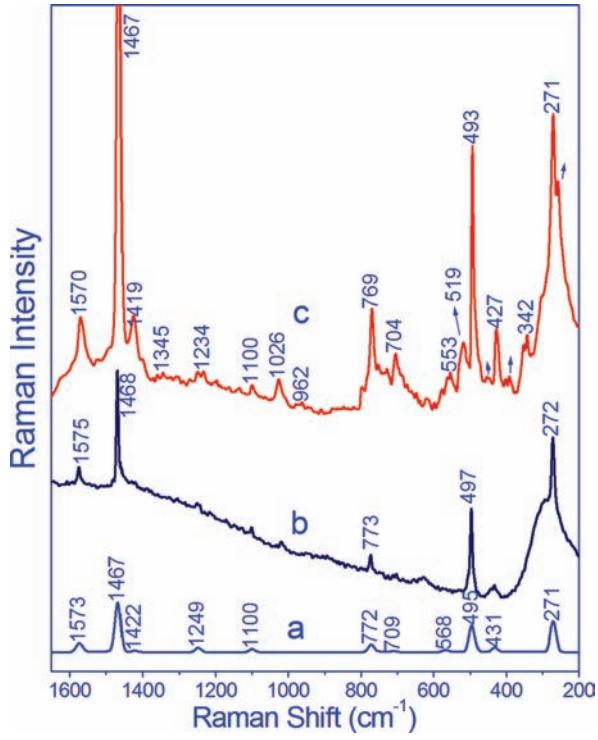

Figure 3. (a) FT-Raman of solid C_{60} powders, (b) Raman of C_{60} nanotubes arrays supported in the pores of AAO templates, and (c) SERS from the Au@C_{60} nanopillar arrays system. All excited at 1064 nm.

3a, the spectrum of the solid C_{60} nanotube arrays supported on AAO templates shows relative worse signal-to-noise attributed to the strong fluorescence background of the alumina frame. In the case of the spectrum of the nanopillar arrays (Figure 3c), besides the 10 normal Raman modes of C_{60} with frequencies at 271, 431/427, 495/493, 709/704, 772/769, 1100, 1249/1234, 1422/1419, 1467, and 1573/1570 cm^{-1}, there are many more sharp peaks that refer to the appearance of some nonactive Raman modes or additional modes of C_{60}. (See Table 1.)

The very high symmetry of the C_{60} cluster poses serious problems for a complete identification of the 46 normal modes ($2A_g + 8H_g + 4T_{1u} + 3T_{1g} + 4T_{2g} + 6G_g + A_u + 5T_{2u} + 6G_u + 7H_u$) and their corresponding frequencies. In the I_h symmetry group, only 10 normal modes are Raman ($2A_g + 8H_g$) active ($4T_{1u}$ are infrared active). Here the FT-Raman spectrum clearly reproduces the 10 Raman modes. For the Au−C_{60} complex, however, symmetry reduction in this complex allows additional vibrational modes to become Raman-active.[23] By far, the four T_{1u} infrared active and the remaining 32 silent modes ($3T_{1g} + 4T_{2g} + 6G_g + A_u + 5T_{2u} + 6G_u + 7H_u$) have been reported to appear in relative SERS bands.[24] The Raman spectrum from the Au@C_{60} core−shell nanopillar arrays actually presents similarity to the optimized SERS of C_{60} (Figure S4 in the Supporting Information). According to the SERS mechanism, the enhancement is attributed to the absorption and localization of photons by the substrates. For common SERS substrates, their rough surfaces absorb photons and "store" the energy as the surface plasmon. The electromagnetic energy is delocalized in the direction parallel to the surface but localized in the perpendicular one. The high-density and ordered arrays of Au nanopillars have the advantage of increasing the electromagnetic energy density near the surface. In addition, the spacing of Au nanopillars is close to the excitation wavelength and the local field is increased because of the resonance effect, which in turn causes the enhanced dipole moment. This assumption accords with the common knowledge that the high SERS activity is usually ascribed to the symmetry lowering and selection rule relaxation of the probe molecules located near metal substrates.

It is significant that the remarkable enhanced Raman spectrum from the Au@C_{60} nanopillar is also achievable by using an excitation at 514 nm. As shown in Figure 4a, the 514 nm excited Raman spectrum of C_{60} shows poor signal-to-noise because of its strong fluorescence. The Raman spectrum from the Au@C_{60} nanopillar array system shows much better signal-to-noise and many more peaks, especially sharp peaks at the high-frequency region, such as those at 1387, 1468, and 1571 cm^{-1} (Figure 4b). These results indicate that the Au@C_{60} core−shell nanopillar arrays system can effectively quench the fluorescence of

TABLE 1: Assignment of Measured Raman and SERS Bands of C_{60}

solid Raman of C_{60} excited at		SERS of Au@C_{60} excited at		
514 nm	1064 nm	514 nm	1064 nm	assignment
	271	267	252/269	H_g (1)
			342	T_{2u} (1)
			401	Hg (2)
	431	437	427	
	495	494	493	A_g (1)
			519	T_{1u} (1)
	568	564	553	T_{1u} (2)
			578	
	709	709	704	H_g (3)
		726	733	
	772		769	
		858	835	H_g (4)
		970	962	F_{1g} (1)
			1026	T_{2u} (1)
	1100		1100	H_g (5)
		1130	1147	
		1197	1184	G_g
			1234	T_{1u} (3)
	1249	1242	1269	H_g (6)
		1347	1345	
		1387	1378	F_{1g}
	1422	1429	1419	
1456	1467	1468	1467	H_g (7)/T_{1u} (4)
		1503	1503	A_g (2)
1586	1573	1571	1570	H_g (8)

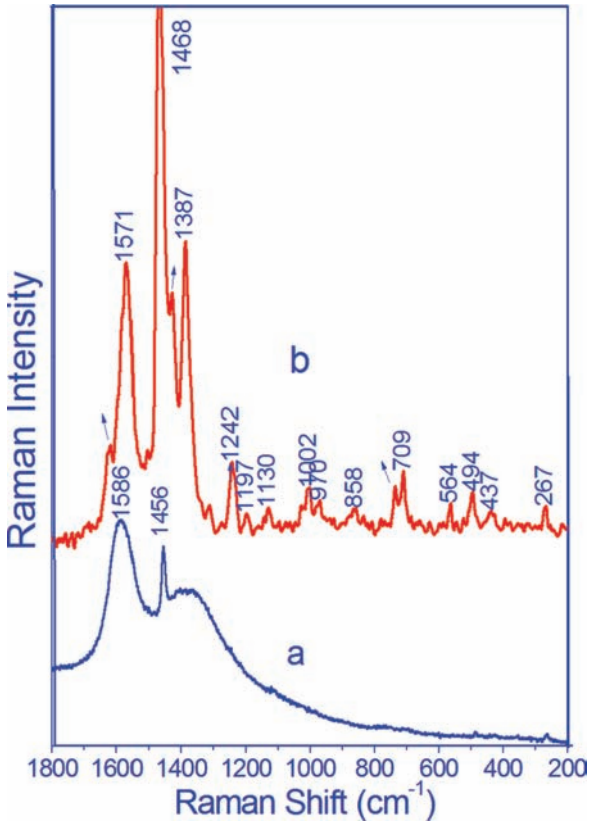

Figure 4. SERS spectra of (a) solid fullerene C_{60} and (b) the Au@C_{60} nanopillar array system. The excitation wavelength was at 514 nm.

C_{60}, which is considered to be the dominant contribution to the SERS enhancement in this system. The evidence of fluorescence quenching is also directly given by fluorescence emission spectra for Au−C_{60} nanorodding separated in NaOH solution (Figure S5 in the Supporting Information).

It needs to be mentioned that the Au nanoparticles usually can only generate remarkable surface plasmon resonance with a near-infrared excitation, but rare resonance is achieved with UV−vis excitation. It is likely that the arrays of Au@C_{60} core−shell nanopillars supported by the AAO template is a good system to gain enhanced Raman for fluorescence molecules. The new system actually includes a consideration of the molecular assembly and enhanced surface plasmon effect,[25,26] where the nanotubes of fullerene C_{60} hold Au nanoparticles in the tube-hole to act as plasmon sources. When the C_{60} molecules were orderly assembled along the pipe-wall of the AAO pores to form standing nanotubes with Au-rod cores, the Raman response may be greatly increased because of the combined contribution of these uniform molecules. If the adsorption of C_{60} occurred on spherical Au nanoparticles as usual SERS, then the random arrangement of the molecules should induce an arbitrary orientation of the dipoles. It is assumed that the high density ordered arrays of Au@C_{60} nanopillars induce a stronger surface plasmon resonance effect at the tips of the nanopillars than the Au colloidal nanoparticles.

It should be mentioned that the penetration of the laser light is actually greater than the average measurement from disordered aggregated Au@fullerene clusters because the as-prepared AAO templates are transparent. By a similar approach, C_{70} nanotubes (Figure 5a) and the Au@C_{70} system (Figure 5b−d) were also fabricated. The remarkable SERS from the Au@C_{70} nanopillar arrays system was also observed. Compared with the solid Raman spectrum, the Au@C_{70} system shows many more sharp

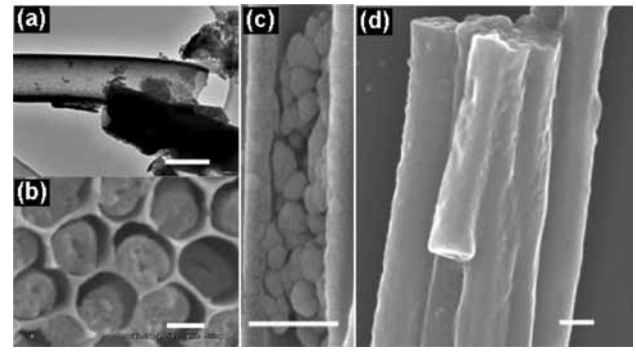

Figure 5. (a) TEM images of C_{70} nanotubes. (b) SEM images of the Au@C_{70} nanorods before dissolving AAO template frame. (c) SEM image for the inner morphologies of an Au@C_{70} nanorod operated with microtomy technique and (d) stacks of several separated Au@C_{70} nanorods removed from the AAO and separated on silicon. The dimension bars are 200 nm for all.

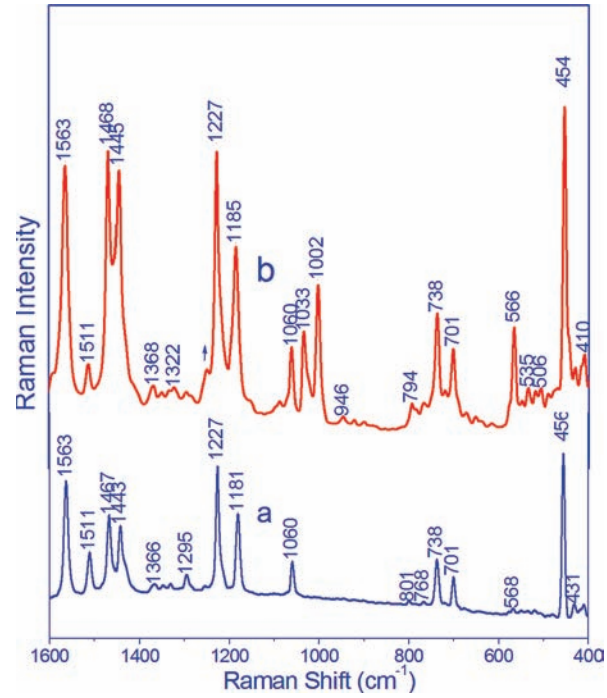

Figure 6. (a) FT-Raman of solid C_{70} and (b) enhanced Raman of fullerene C_{70} from the Au@C_{70} nanopillar arrays system excited at 1064 nm.

peaks appearing in relative bands, in both the high- and low-frequency regions, as shown as Figure 6.

Recently, many groups have hammered at the argument that the largest enhancement factors typically occur in junctions between coupled nanoparticles when illuminated by light polarized across the junction between the particles.[27−30] They demonstrated that the particle junctions, when illuminated by light of a wavelength in resonance with the coupled nanoparticle plasmon induced by the intense electric fields, are believed to be the "hot-spots" for Raman scattering, which dominates the observed SERS signal in more complex nanoparticle aggregates. Recent advances have also shown that a strong electromagnetic field is invoked not only between solid nanoparticles, such as colloids, but also at sharp boundaries of nanoscale geometries, such as on island films and gratings,[31,32] as well as an ordered array of geometric nanoscale features.[33−38] The as-prepared high-density ordered arrays of core−shell nanopillars of Au@C_{60}/C_{70} are actually operated by optimizing Raman active "hot-

spots" with molecules uniformly assembled instead of with random location.[18]

4. Conclusions

Employing a two-step approach of infiltration (for C_{60}/C_{70} solution) and pressure-difference approach (for Au colloid), we fabricated high-density ordered arrays of core−shell nanopillars of $Au@C_{60}/C_{70}$. High-quality SERS spectra of fullerene C_{60}/C_{70} were obtained. The spectra show intense SERS signals with a fluorescence-free background, even with a 514 nm excitation by which normal Raman present poor signal-to-noise. The results suggested that the coincident and uniform assembled orientation of C_{60} molecules along the Au nanorods led to fluorescence quenching, and the high-density and ordered arrays of nanopillars bring forth surface plasmon resonance in achieving the enhancement in the Raman scattering.

Acknowledgment. This work was supported by the National Natural Science Foundation of China (nos. 20733006 and 50720145202), the CAS/SAFEA International Partnership Program for Creative Research Teams, and the National Research Fund for Fundamental Key Project 973 (2006CB806200).

Supporting Information Available: Characterization of the fabricated AAO templates, sketch for the fabrication of $Au@C_{60}/C_{70}$, usual SERS of C_{60}, fluorescence spectra, and Raman modes of Fullerene C_{70} obtained in this work and their symmetry assignments. This material is available free of charge via the Internet at http://pubs.acs.org.

References and Notes

(1) Birkett, P. R. *Annu. Rep. Prog. Chem., Sect. A: Gen., Phys., Inorg. Chem.* **2000**, *96*, 467.
(2) Hou, J. G.; Jinlong, Y.; Haiqian, W.; Qunxiang, L.; Changgan, Z.; Lanfeng, Y.; Bing, W.; Chen, D. M.; Qingshi, Z. *Nature* **2001**, *409*, 304.
(3) Janda, P.; Krieg, T.; Dunsch, L. *Adv. Mater.* **1998**, *10*, 1434.
(4) Shirai, Y.; Cheng, L.; Chen, B.; Tour, J. M. *J. Am. Chem. Soc.* **2006**, *128*, 13479.
(5) Liu, H.; Li, Y.; Jiang, L.; Luo, H.; Xiao, S.; Fang, H.; Li, H.; Zhu, D.; Yu, D.; Xu, J.; Xiang, B. *J. Am. Chem. Soc.* **2002**, *124*, 13370.
(6) Liu, P.; Zhang, Y. W.; Lu, C. *J. Appl. Phys.* **2005**, *97*, 094313.
(7) Verberck, B.; Michel, K. H. *Phys. Rev. B* **2006**, *74*, 045421.
(8) Deng, F. J.; Yang, Y. Y.; Hwang, S.; Shon, Y. S.; Chen, S. W. *Anal. Chem.* **2004**, *76*, 6102.
(9) Kröger, H.; Reinke, P.; Büttner, M.; Oelhafen, P. *J. Chem. Phys.* **2005**, *123*, 114706.
(10) Lim, I. I. S.; Ouyang, J.; Luo, J.; Wang, L. Y.; Zhou, S. Q.; Zhong, C. J. *Chem. Mater.* **2005**, *17*, 6528.
(11) Sudeep, P. K.; Ipe, B. I.; Thomas, K. G.; George, M. V.; Barazzouk, S.; Hotchandani, S.; Kamat, P. V. *Nano Lett.* **2002**, *2*, 29.
(12) Lahav, M.; Weiss, E. A.; Xu, Q. B.; Whitesides, G. M. *Nano Lett.* **2006**, *6*, 2166.
(13) Daly, B.; Arnold, D. C.; Kulkarni, J. S.; Kazakova, O.; Shaw, M. T.; Nikitenko, S.; Erts, D.; Morris, M. A.; Holmes, J. D. *Small* **2006**, *2*, 1299.
(14) Al-Kaysi, R. O.; Dillon, R. J.; Zhu, L. Y.; Bardeen, C. J. *J. Colloid Interface Sci.* **2008**, *327*, 102.
(15) Kneipp, K.; Kneipp, H.; Itzkan, I.; Dasari, R. R.; Feld, M. S. *Chem. Rev.* **1999**, *99*, 2957.
(16) Moskovits, M. *Rev. Mod. Phys.* **1985**, *57*, 783.
(17) Schatz, G. C.; Young, M. A.; Van Duyne, R. P. *Top. Appl. Phys.* **2006**, *103*, 19.
(18) Luo, Z.; Peng, A.; Fu, H.; Ma, Y.; Yao, J.; Loo, B. H. *J. Mater. Chem.* **2008**, *18*, 133.
(19) Moskovits, M. *Rev. Mod. Phys.* **1985**, *57*, 783.
(20) Frens, G. *Nature Phys. Sci.* **1973**, *241*, 20.
(21) Luo, Z. X.; Fang, Y. *J. Comb. Chem.* **2006**, *8*, 500.
(22) Luo, Z.; Liu, Y.; Kang, L.; Wang, Y.; Fu, H.; Ma, Y.; Yao, J.; Loo, B. H. *Angew. Chem., Int. Ed.* **2008**, *47*, 8905.
(23) Luo, Z. X.; Fang, Y. *J. Colloid Interface Sci.* **2005**, *283*, 459.
(24) Schettino, V.; Pagliai, M.; Cardini, G. *J. Phys. Chem. A* **2002**, *106*, 1815.
(25) Schull, G.; Berndt, R. *Phys. Rev. Lett.* **2007**, *99*, 226105.
(26) Shpilevskii, E. M.; Zamkovets, A. D. *J. Opt. Technol.* **2008**, *75*, 298.
(27) Michaels, A. M.; Jiang, J.; Brus, L. E. *J. Phys. Chem. B* **2000**, *104*, 11965.
(28) Sawai, Y.; Takimoto, B.; Nabika, H.; Ajito, K.; Murakoshi, K. *J. Am. Chem. Soc.* **2007**, *129*, 1658.
(29) Xu, H. X.; Aizpurua, J.; Kall, M.; Apell, P. *Phys. Rev. E* **2000**, *62*, 4318.
(30) Xu, H. X.; Bjerneld, E. J.; Kall, M.; Borjesson, L. *Phys. Rev. Lett.* **1999**, *83*, 4357.
(31) Dick, L. A.; McFarland, A. D.; Haynes, C. L.; Van Duyne, R. P. *J. Phys. Chem. B* **2002**, *106*, 854.
(32) Chou, I.-H.; Benford, M.; Beier, H. T.; Coté, G. L.; Wang, M.; Jing, N.; Kameoka, J.; Good, T. A. *Nano Lett.* **2009**, *8*, 1729.
(33) Billot, L.; Lamy de la Chapelle, M.; Grimault, A.-S.; Vial, A.; Barchiesi, D.; Bijeon, J.-L.; Adam, P.-M.; Royer, P. *Chem. Phys. Lett.* **2006**, *422*, 303.
(34) Félidj, N.; Aubard, J.; Lévi, G.; Krenn, J. R.; Salerno, M.; Schider, G.; Lamprecht, B.; Leitner, A.; Aussenegg, F. R. *Phys. Rev. B* **2002**, *65*, 075419.
(35) Siiman, O.; Ledis, S. *J. Raman Spectrosc.* **2005**, *36*, 1125.
(36) Wang, H. H.; Liu, C. Y.; Wu, S. B.; Liu, N. W.; Peng, C. Y.; Chan, T. H.; Hsu, C. F.; Wang, J. K.; Wang, Y. L. *Adv. Mater.* **2006**, *18*, 491.
(37) Yu, Q.; Guan, P.; Qin, D.; Golden, G.; Wallace, P. M. *Nano Lett.* **2008**, *8*, 1923.
(38) Zhao, Y. P.; Chaney, S. B.; Shanmukh, S.; Dluhy, R. A. *J. Phys. Chem. B* **2006**, *110*, 3153.

JP9041028